Available online at www.sciencedirect.com
SCIENCE DIRECT®
Organic Electronics 4 (2003) 165–177
Organic Electronics
www.elsevier.com/locate/orgel

Fluorene-based conjugated polymer optical gain media

Ruidong Xia, George Heliotis, Yanbing Hou, Donal D.C. Bradley *

Ultrafast Photonics Collaboration, Experimental Solid State Group & Centre for Electronic Materials and Devices, Blackett Laboratory, Imperial College London, Prince Consort Road, London SW7 2BZ, UK

Abstract

We report a detailed investigation of the optical gain properties of a series of semiconducting polyfluorenes with photoluminescence emission spectra that span the entire visible spectrum. Stimulated emission was demonstrated at low pump pulse energies ($\geqslant 0.1$ μJ for 10 ns, 10 Hz pulses) in the blue, green and red parts of the spectrum via amplified spontaneous emission (ASE) measurements on asymmetric slab waveguides. These structures exhibit large net gains $g \leqslant 74$ cm^{-1}, and corresponding gain cross-sections $\sigma \geqslant 7 \times 10^{-16}$ cm^2, together with very low loss coefficients, $\alpha \geqslant 3.2$ cm^{-1}. The spectral location of the maximum waveguide amplification can be widely tuned ($\Delta\lambda \geqslant 30$ nm) by controlling the allowed propagating modes or by blending the active emitter with a second larger optical gap polyfluorene. Our results confirm that fluorene-based polymers are attractive gain media for use in highly tuneable solid-state polymer lasers and amplifiers.

1. Introduction

The demonstration of stimulated emission in conjugated polymers makes these materials promising as high gain media for solid-state lasers [1–3]. Some of the unique optical properties that make conjugated polymers attractive candidates for such applications are their high photoluminescence quantum efficiencies (PLQE), large stimulated emission cross-sections and chemically tuneable emission wavelengths [4–6]. To date, optically pumped lasers based on conjugated polymers have been demonstrated in both solution and thin films, and in resonators based on simple waveguides or more sophisticated structures using distributed feedback geometries, photonic crystals and microrings [7–11]. Considerable efforts are being made to improve the intrinsic carrier mobilities in these materials and lower their lasing thresholds in order to progress towards electrically pumped polymer laser diodes [12,13]. Such organic laser sources may eventually compete with inorganic semiconductor lasers in a number of fields, especially if the benefits of low-cost, low-temperature, high throughput manufacture on a variety of substrates can be attained. Semiconducting conjugated polymers exhibit optical gain over broad spectral ranges, offering potential applications in highly tuneable lasers and broadband amplifiers [14,15].

In this paper, we report a detailed investigation of the optical gain properties of four semiconducting polyfluorenes with chemically tuned emission characteristics that span the spectral range from 400 to 800 nm. We demonstrate low

* Corresponding author. Tel.: +44-20-75947612; fax: +44-20-75813817.
E-mail address: d.bradley@imperial.ac.uk (D.D.C. Bradley).

1566-1199/$ - see front matter © 2003 Elsevier B.V. All rights reserved.
doi:10.1016/j.orgel.2003.08.009

threshold light amplification in the blue, green and red via stripe-pumped, amplified spontaneous emission (ASE) measurements on asymmetric slab waveguides (formed by spin coating polymer films on top of synthetic quartz substrates). ASE leads to a rapid growth of the output light intensity at the maximum gain position and a collapse in the total linewidth of the emission from ~100 nm to a few nm. The wavelength at which amplification occurs can be widely tuned: this can be done by altering the slab waveguide thickness to control the allowed modes and/or by modifying the refractive index, emission spectrum and PLQE of the active material via blending with a second, larger optical gap "host" polyfluorene. Our observations highlight the broad spectral range for gain that is accessible with these materials. We report the net gain, g, and loss, α, characteristics of the polymer waveguides that we have studied and calculate the corresponding effective gain cross-sections, σ. Finally, we calculate the refractive indices of the active layers using the slab waveguide cut-off thicknesses for light propagation at the maximum gain wavelength.

We note that polyfluorenes also offer excellent charge transport properties [16] and are thus of strong potential interest for electrically pumped devices [17,2]. However, it is important to recognise that the fabrication of laser diodes based on thin films of organic semiconductors still represents a major challenge for research and development. Amongst the identified issues that lead to additional problems in structures that are suitable for electrical pumping, are optical losses due to: (i) the proximity of the emissive region to the electrodes, (ii) the intra-gap absorption peaks of charge states, and (iii) the intra-gap absorption peaks of triplet states [4,6,18,19]. Low charge carrier mobilities play an important rôle here as they make lateral separation of the carrier injection and optical gain regions very difficult: Carriers do not transport effectively across distances that are large compared to the optical confinement dimensions. In addition, low mobilities limit the inter-electrode separation for acceptable driving voltages (transport is field dependent), with the result that there are relatively strong interactions between in-plane propagating modes and the electrodes. Intra-gap absorption reduces net gain and potentially leads to instability (via excitation of higher lying states). Charged states can also be stabilized by the same disorder that gives rise to low mobilities, leading to lifetimes of tens to hundreds of μs. Triplet states, expected to be more significant under electrical- than optical-pumping (due to the non-geminate pair recombination that dominates in the former case), have similarly long lifetimes and can, via energy transfer, lead to the excitation of molecular oxygen into its highly reactive, singlet excited state. The lesson, in this context, from the development of dye lasers is that, ideally, sufficient time needs to be allowed to elapse between sequential excitation events in order that the triplet states are able to decay. For a dye laser this equates with the use of a circulator that takes the dye around an extended flow path before re-entering the pumping region. This is not necessarily so easy to achieve for a solid-state laser. However, how closely these, reportedly, general features of organic lasers map onto specific conjugated polymer systems and device structures remains to be established. The above issues have not yet been addressed in detail for the materials that are the subject of this paper. Thus, whilst better characterization and understanding of the limitations of optically pumped structures, as described below, represents an important move in the right direction, it does not present a solution to the problem of achieving an electrically pumped laser. Additional work will be needed to carefully address the factors that play a specific rôle in electrically pumped structures: This is the subject of on-going research.

2. Sample fabrication and experimental procedures

The conjugated polymers that we have investigated were synthesized and carefully purified at The Dow Chemical Company. In particular, we have studied the blue emitting poly(9,9-dioctylfluorene) [PFO] and poly(9,9-dioctylfluorene-*co*-9,9-di(4-methoxy)phenylfluorene [F8DP], the green emitting poly(9,9-dioctylfluorene-*co*-benzothiadiazole) [F8BT], and the Dow proprietary red emission copolymer known as Dow Red F. Planar

waveguides were made by spin-coating 35–350 nm thick films from 20 mg/ml toluene (for F8DP, F8BT and Dow Red F) or *p*-xylene (for PFO) solutions onto polished synthetic quartz (Spectrosil B) substrates. The film thicknesses were measured with a Dektak Surface Profilometer. Absorption measurements were performed using a Unicam IV UV–Vis spectrophotometer. Photoluminescence (PL) spectra were measured on the same samples using a monochromated Xe lamp as excitation source, and the emitted light collected with a fibre bundle and dispersed in a spectrograph with a charge-coupled device (CCD) detector. Quantitative measurements of the PL quantum efficiency were obtained using an integrating sphere [20,21] attachment in a Spex FluoroMax 3 fluorimeter. We have also measured the time resolved photoluminescence decays for these polymers using a Hamamatsu Photonics Streakscope, following excitation with a 409 nm pulsed laser diode (pulse width 66 ps, repetition rate 1 MHz). Further PL decay results are reported elsewhere [22].

For gain measurements, the samples were optically pumped with a Q-switched, neodymium ion doped yttrium aluminium garnate [Nd^{3+}:YAG] laser pumped, type-II β-BaB_2O_4 [BBO], optical parametric oscillator that delivered 10 ns pulses at a repetition rate of 10 Hz. The pump wavelength was chosen to match the absorption maxima of the individual polymers (see Fig. 1(a)). The pulse energy incident on the sample was adjusted by the insertion of calibrated neutral density filters into the beam path. The pump beam was focused with a cylindrical lens and spatially filtered through an adjustable slit, to create a narrow 400 μm × 4 mm, excitation stripe on the sample. At sufficient excitation intensities, the spontaneously emitted photons that are waveguided along the stripe-shaped gain region are amplified via stimulated emission. This results in most of the light being emitted from the ends of the stripe. For this reason, we placed one end of the stripe right up the edge of the film and collected the emission with a fibre bundle. The output from the fibre bundle was in turn, focused into a grating spectrograph, wavelength dispersed and then detected with a CCD detector.

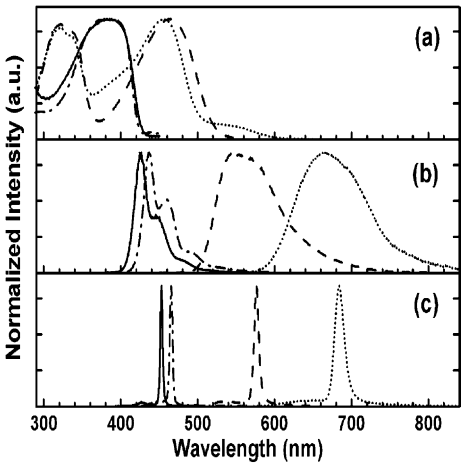

Fig. 1. Normalized (a) absorption, (b) photoluminescence and (c) ASE spectra measured on F8DP (—), PFO (-·-·-·), F8BT (- - -) and Dow Red F (···) slab waveguide structures.

The approach we followed to investigate the net material gain is the variable stripe length (VSL) method. It is commonly used to characterize both inorganic and organic semiconductors in slab geometry [23,24]. In brief, it involves optical pumping of the sample with a stripe of variable length and measurement of the intensity of the edge-emitted light as a function of the stripe length. The net gain coefficient, g, was then determined by fitting the resulting curves to the expected dependence for ASE in the small-signal regime:

$$I_{\text{out}}(\lambda) = \frac{AP_0}{g(\lambda)}[\exp(g(\lambda)l) - 1], \tag{1}$$

where I_{out} is the intensity of the edge-emitted light and l the length of the stripe. The VSL, edge-emitted, intensity characteristics were found to be identical when scans were taken from low to high pump energies and vice versa, indicating that degradation was not a significant issue. It is also worth noting that the characteristics measured in air exhibited the same behaviour as those measured at $\approx 10^{-2}$ mbar in a vacuum chamber, which again can be interpreted as a signature of the high thermal and photoxidative stability of the polyfluorenes that we have studied. It is interesting to note here that CW excitation often leads to photoxidation. This is readily seen in the dioctylfluorene

homopolymer by the accompanying appearance of a broad and featureless, fluorenone photoproduct related, excimer emission, to the red of the normal intra-chain blue emission [25]. The relative stability under intense pulsed light compared to CW irradiation is intriguing and suggests that triplet states play a rôle in photoxidation: The pulsed measurements are undertaken with a low repetition rate (10 Hz) which allows adequate time between sequential pulses for the triplets to decay.

To more fully characterize our structures, we also measured the waveguide losses. In these experiments we kept the length of the pump stripe fixed but gradually translated it away from the sample edge. Since the emission from the end of the pump stripe I_0 can be assumed to be constant (fixed stripe length), the emission from the edge of the sample should decrease as a result of the waveguide losses (absorption and scattering of emitted radiation out of the guide) that occur during propagation across the unpumped region. The detected output intensity, I_{out}, can be expressed as

$$I_{out} = I_0 \exp(-\alpha x), \tag{2}$$

where x is the length of the unpumped region between the end of the pump stripe and the edge of the sample and α is a combined waveguide loss coefficient.

3. Experimental results

Fig. 1 shows (a) the absorption and (b) the photoluminescence spectra of the four polymers that we have studied. The measurements were made on 120 nm (for PFO and F8DP), 180 nm (for F8BT) and 250 nm (for Red F) thickness films spin-coated on polished spectrosil B discs. The PL spectra were obtained by exciting the samples at 340 nm for PFO, F8DP and F8BT, and at 440 nm for Dow Red F. The absorption and PL spectra of F8DP (solid lines) and PFO (dash-dotted lines) are very similar, exhibiting a featureless absorption band that peaks at 390 nm and a structured emission band. However, the PL emission of F8DP shows a ~15 nm blue-shift compared to that of PFO and a greater weight in the lower vibronic levels, and therefore, a smaller Huang–Rhys parameter. An additional difference between the two blue-emitting materials is that F8DP is not prone to the polymorphism that characterises PFO [16,26,27]. Hence, F8DP films of different thickness, prepared from different solvents, all show the same spectral characteristics: This is clearly advantageous from a device production perspective as it increases the fabrication parameter space that can be accessed without altering the material properties. The absorption spectra of both F8BT (dashed lines) and Dow Red F (dotted lines) show maxima at about 330 and 455 nm. However, the spectra are distinguishable by the weaker, long wavelength absorption feature at 550 nm and the shoulder at 400 nm, both of which appear for Dow Red F but not F8BT. The former feature arises from the presence of the red chromophore units in the polymer backbone. Although the absorption spectra of F8BT and Dow Red F have strong similarities, the PL spectra of these two materials span quite different spectral ranges. We note further that the PL spectra of Red F exhibit exactly the same profile when the polymer is excited at each of the three main, long wavelength absorptions ($\lambda = 340$, 455 and 550 nm). This implies that the red chromophore units play the key role in the emission of Dow Red F with efficient energy transfer from the higher lying states. The PL of these four polymers covers the range 400 to 800 nm, illustrating the potential for fluorene-based polymer gain media to span the full visible spectrum.

A quantitative measure of the external PL efficiency [PLQE] shows that the PLQE values are typically $50 \pm 5\%$ for F8DP and PFO at $\lambda_{ex} = 355$ nm, $58 \pm 5\%$ for F8BT at $\lambda_{ex} = 440$ nm and $40 \pm 5\%$ for Dow Red F at $\lambda_{ex} = 532$ nm. We have also measured the time resolved photoluminescence decays for these polymers. Fig. 2 shows the PL decay curves for the four polyfluorene derivatives. All curves can be fit with reasonable accuracy to a monoexponential decay, from which the singlet excited state lifetimes (τ) can be estimated. We find $\tau = 352$, 227, 2028 and 2725 ps for F8DP, PFO, F8BT and Dow Red F respectively.

We have investigated the gain characteristics of the four polymers via ASE measurements para-

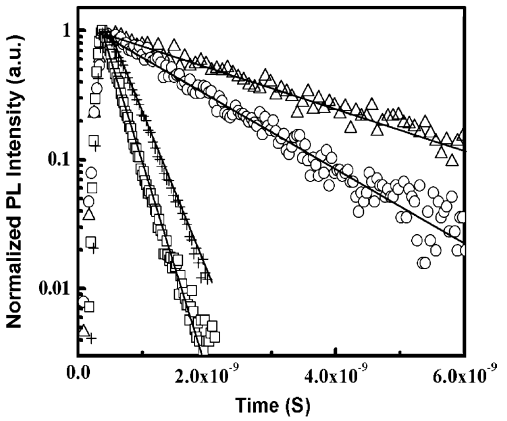

Fig. 2. PL dynamics of F8DP (×), PFO (□), F8BT (○) and Dow Red F (△). Solid lines are single exponential fits.

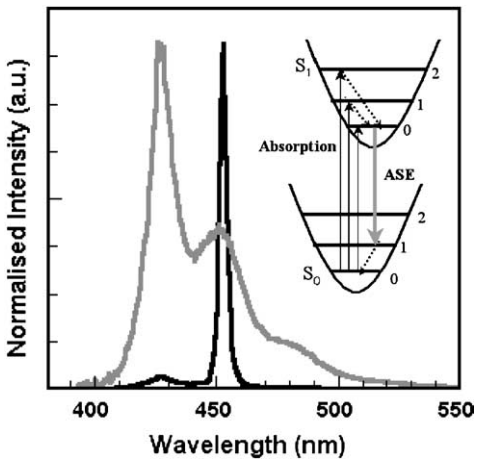

Fig. 3. Emission spectra of the F8DP waveguide below (grey line) and above the ASE threshold (black line). Inset is the corresponding simplified vibronic-level diagram.

metric in excitation pulse energy. The pump wavelengths were chosen, in each case, to be close to the peaks in the absorption spectra of each polymer, namely $\lambda_{ex} = 355$ nm for F8DP; 390 nm for PFO; 337 and 440 nm for F8BT; and 337, 440 and 532 nm for Dow Red F. Fig. 1(c) presents the combined ASE spectra of F8DP (140 nm thickness, solid line), PFO (130 nm thickness, dash-dotted line), F8BT (180 nm thickness, dashed line) and Dow Red F (300 nm thickness, dotted line) slab waveguides at pump pulse energies of 2.0, 1.6, 5.0 and 5.5 μJ respectively. ASE occurs at the 0–1 vibronic peak of the PL emission (most readily seen for the well-structured PL spectra of F8DP and PFO) consistent with a quasi-four-vibronic-level gain process that should allow low threshold lasing [28]. Results for F8DP are shown in Fig. 3 together with a schematic vibronic level diagram, that illustrates absorption (vertical arrows) from the lowest vibronic level of the ground state to the $v = 0$, 1 and 2 vibronic levels of the S_1 excited state. Internal conversion (dotted line arrows) and subsequent stimulated emission (ASE) from the lowest vibronic levels of the S_1 excited state to the $v = 1$ vibronic levels of the S_0 ground state is also indicated.

The same gain phenomena were observed for each of the four polymers that we studied: At low laser pump pulse energies (e.g., $E \leqslant 0.06$ μJ for F8DP) the emission spectra, as expected, match closely the PL spectra measured under low power CW excitation (Fig. 1(b)). As the pulse energy increases, the emission spectra change drastically: A sharp ASE peak becomes apparent and grows to dominate the spectrum. The ASE peaks were observed at 452, 466, 576 and 685 nm respectively for the F8DP, PFO, F8BT and Dow Red F slab waveguides that we studied. ASE does not strictly have a threshold. However, in order to quantify our observations we define a threshold pulse energy, E_{th}, at which the full width at half maximum [FWHM] linewidth of the emission drops to half its low energy excitation PL value. This energy is usually also accompanied by a kink in the input versus output intensity graphs of the waveguides. The deduced E_{th} values are listed in Table 1 together with the corresponding pump wavelengths, ASE wavelengths and ASE FWHM linewidths.

In order to more fully understand the ASE characteristics of F8BT and Dow Red F we have investigated their excitation wavelength dependences by pumping at the different peaks (or shoulders) that appear in their absorption spectra. The inset to Fig. 4 shows the normalised ASE spectra obtained by stripe-pumping Dow Red F slab waveguides at three different wavelengths, namely 337, 440 and 532 nm. We note that the pulse energy was about 40 μJ when exciting at 337 nm while it was 5.6 μJ in the other two cases. The stripe configuration was the same in all three cases.

Table 1
The optical gain related parameters extracted from our measurements on four fluorene-based conjugated polymers: λ_{ASE}, E_{th}, ASE FWHM and $\Delta\lambda_{ASE}$ are the ASE wavelength, threshold pump energy, ASE linewidth well above threshold and demonstrated ASE wavelength tuning range for slab waveguide structures when optically pumped at λ_{ex}; $g_{net,max}$ is the maximum measured net gain coefficient, and α the waveguide loss coefficient. Also listed are the photoluminescence quantum efficiencies (PLQE), lifetimes for the emissive singlet excited states (τ), waveguide cut-off thicknesses for propagation at the maximum gain wavelength (d_c) and corresponding refractive indices (n), saturation energy densities (E_S/A) and corresponding gain cross-sections (σ)

Polymers	F8DP	PFO	F8BT	Red F
λ_{ex} (nm)	355	390	440	532
λ_{ASE} (nm)	452	466	576	685
E_{th} (μJ)	0.1	0.35	0.45	0.45
ASE FWHM (nm)	5	5	8	10
$\Delta\lambda_{ASE}$ (nm)	18	20	17	25
$g_{net,max}$ (cm^{-1})	66	74	22	24
α (cm^{-1})	14.8	3.5	7.6	3.2
PLQE (%)	50 ± 5	50 ± 5	58 ± 5	40 ± 5
τ (ps)	352	227	2028	2725
d_c (nm)	66 ± 5	70 ± 5	100 ± 7	140 ± 7
n	1.75	1.72	1.69	1.65
E_S/A (10^{-4} J/cm^2)	6.69	5.63	4.86	3.75
σ (10^{-16} cm^2)	6.57	7.58	7.09	7.73

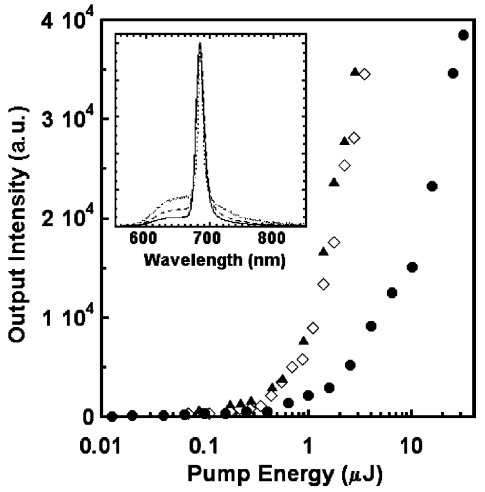

Fig. 4. Edge emitted output intensity at the ASE wavelength for Dow Red F as a function of excitation energy at $\lambda_{ex} = 337$ nm (●), 440 nm (▲) and 532 nm (◇). The inset shows the ASE spectra of the Dow Red F waveguide obtained by pumping at $\lambda_{ex} = 337$ nm (···), 440 nm (- - -) and 532 nm (—). The pump energies were 40 μJ for $\lambda_{ex} = 337$ nm and 5.5 μJ for $\lambda_{ex} = 440$ nm and 532 nm, respectively.

ASE is clearly operative for all three, pump wavelengths but differing relative amounts of background spontaneous emission are evident. The normalised spectra show a continuous reduction in the spontaneous emission (peaked at $\lambda = 650$ nm) as the pump wavelength is shifted from 337 nm to 440 nm to 532 nm. Specifically, the ratios of the integrated areas for the ASE emission and the spontaneous emission background are found to be 1.10 when $\lambda_{ex} = 337$ nm, 2.21 when $\lambda_{ex} = 440$ nm and 3.55 when $\lambda_{ex} = 532$ nm. There is also a slight red-shift of the ASE peak that we consider may be due to more effective ground state saturation when the red chromophore is directly pumped. Fig. 4 also shows the pump pulse, energy dependence of I_{out} (measured at the peak ASE wavelength) for each of the three pump wavelengths. The pump energy axis (abscissa) has been plotted on a logarithmic scale to allow the differences in behaviour to be more clearly distinguished. I_{out} rose more rapidly when the Dow Red F slab waveguide was pumped at 440 nm and 532 nm than when pumped at 337 nm. The pump wavelength dependence observed for the F8BT slab waveguides was very similar to that for Dow Red F waveguides. When the pump wavelength shifted from 337 nm to 440 nm, the value of E_{th} decreased from 1.1 μJ to 0.45 μJ. This corresponds

to a power density decrease from 6.6 kW/cm^2 to 2.8 kW/cm^2. [1]

We have found two means by which to further reduce the E_{th} value of our polymer waveguides. The first involves making use of the anisotropic electronic structure that is characteristic of a conjugated polymer chain. This facilitates emission dipole orientation [29] and the generation of substantial dielectric anisotropy [30] provided the polymer chains can be well aligned. We observed a 50% reduction in E_{th} for oriented, glassy nematic PFO slab waveguides within which a high degree of homogeneous (in-plane) polymer chain alignment had been generated by annealing on top of a rubbed polyimide alignment layer [31]. When pumped with light polarised parallel to the chain orientation direction and for a stripe orientation perpendicular to the chain direction the E_{th} value was 0.48 μJ. This compares with a value of 0.96 μJ for the corresponding isotropic control sample.

The second means to reduce the E_{th} value is to disperse Dow Red F at different concentrations within an F8BT matrix. The E_{th} value for excitation at 440 nm decreased from 0.45 μJ for pure Dow Red F to about 0.05 μJ for 10–20% by weight of Dow Red F in the blend. Samples with 5%, 10%, 20%, 30%, 40% and 100% Dow Red F by weight were studied and the lowest threshold was obtained for blends with 10%–30% Dow Red F and correspondingly 90%–80% F8BT. The E_{th} values of all samples are shown in Fig. 5(a). The PL dynamics and PLQE were also measured for these blends. We found that both the excited state lifetimes, τ, and the PLQE values increased when the Dow Red F concentration was gradually decreased from 100% to 5% (see Fig. 5(b)). This implies the presence of unfavourable inter-chain interactions in Dow Red F that limit the gain properties. A detailed investigation of the precise nature of these interactions has not yet been made.

Another interesting phenomenon observed for these blend structures is the significant blue-shift

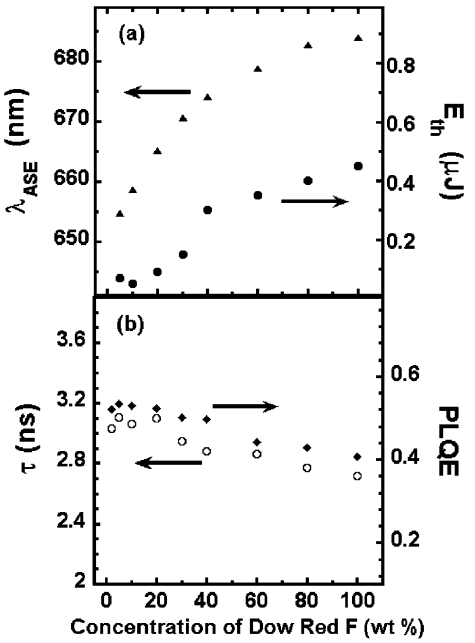

Fig. 5. (a) ASE wavelength (▲, left ordinate) and threshold energy values (●, right ordinate) as a function of Dow Red F wt.% concentration in Dow Red F/F8BT blends. (b) Emission lifetime (○, left ordinate) and PLQE (◆, right ordinate) as a function of Dow Red F concentration.

of the ASE peak wavelength as the fraction of Dow Red F decreases. This effect is shown in Fig. 6 with a $\Delta\lambda \leqslant 30$ nm blue-shift obtained on reducing the Dow Red F fraction to 5% by weight.

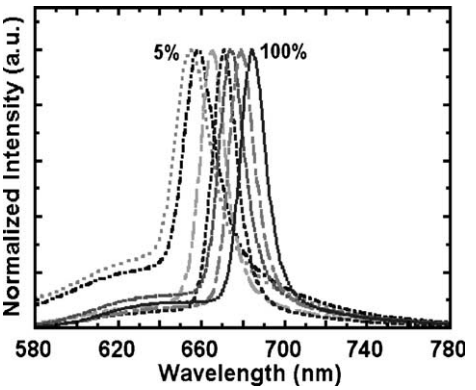

Fig. 6. Wavelength tuning of stimulated emission in F8BT/Dow Red F blend slab waveguides. The two limiting values (5% and 100% Dow Red F) are indicated.

[1] We note that the 10 ns pulse duration of the pump laser is much longer than both the PL and the ASE decay times of the polymers that we have studied. Thus, the system should be under quasi-steady state conditions and the excitation density will then be determined by the pump intensity.

The peak shift is also illustrated in Fig. 5(a). The blue-shift of the ASE peak wavelength could be the result of several factors. First, dilution reduces the net absorption strength of the emitting chromophores and may thus reduce losses at the blue end of the emission spectrum (where spectral overlap occurs between absorption and emission). Second, scattering effects may also be suppressed by dilution, again reducing losses preferentially at shorter wavelengths (λ^{-4} dependence for Rayleigh scattering). A lowering of refractive index at the ASE wavelength due to dilution might also contribute since it would lead to an increase in cut-off thickness, d_c (see Section 4), and therefore to a tendency for the ASE to blue-shift due to the inability of the guide to support a propagating mode at the maximum gain wavelength. The fact that at low loading (5% and 10%), the background spontaneous emission contribution becomes more pronounced might been taken to suggest that the spectral blue-shift is accompanied by an increase in E_{th} but this contradicts the results in Fig. 5(a), where E_{th} continuously decreases on dilution. Further detailed ASE spectral studies on these polymer blend samples are needed to clarify this situation and are currently being undertaken. The initial results will be reported elsewhere [32].

Another way to tune ASE wavelength is to reduce the thickness of the polymer film. ASE narrows the emission spectrum because amplification is maximized within a narrow range of wavelengths for which the highest net gain occurs. In order to support a propagating mode at this wavelength the waveguides need to have a thickness greater than the cut-off thickness, d_c, defined by the refractive indices of the polymer, synthetic quartz substrate and air cladding (see Section 4). The values of the cut-off thickness obtained from direct experimental observations for the four polymer waveguides are given in Table 1. We note that no significant increases in E_{th} values were observed as the thickness of the polymer layer was reduced towards the cut-off value. The cut-off thicknesses of $\leqslant 100$ nm for F8DP, PFO and F8BT thus suggest that the thin films desired for electrically pumped devices can indeed function as high gain structures. Moving to polymer layers that are thinner than the cut-off thickness, forces a blue-shift of the ASE peak. Fig. 7(a) shows the effect of thickness tuning on the ASE spectra of F8DP, F8BT and Dow Red F slab waveguides. The tuning ranges for the ASE wavelengths of the individual polymer waveguides are given in Table 1. The maximum tuning range, $\Delta\lambda \sim 25$ nm was achieved in Dow Red F films by decreasing the active layer thickness from ~140 to ~80 nm. The emitted ASE has TE mode polarization and does not change as the emission blue-shifts. However, as expected, the blue-shift is accompanied by an increase in the ASE threshold. This is apparent in Fig. 7(a) where the normalised spectra (recorded at constant pump energy) show increasing proportions of spontaneous emission: Higher pump energies are needed to cause strong spectral narrowing when the ASE wavelength shifts away

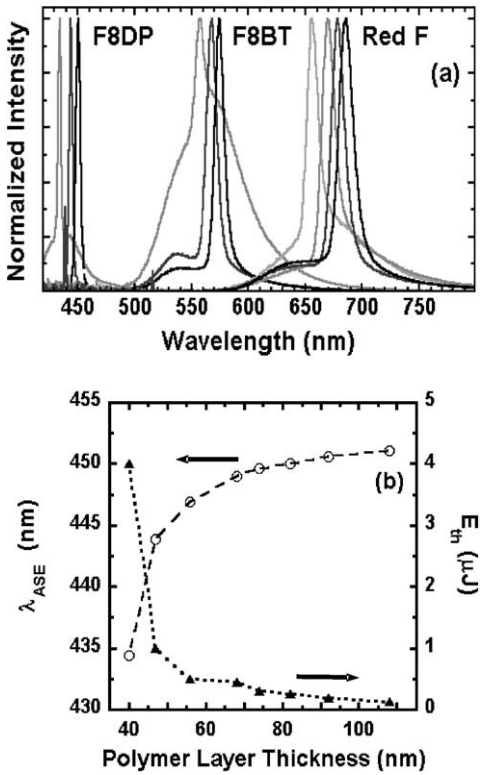

Fig. 7. (a) Thickness dependent ASE spectral shifts for F8DP, F8BT and Dow Red F waveguides. (b) ASE wavelengths (○, left ordinate) and corresponding threshold energies (▲, right ordinate) for a F8DP waveguide as a function of polymer layer thickness.

from the peak of the gain spectrum. Fig. 7(b) shows typical ASE wavelength shifts and changes in threshold energy, E_{th}, for F8DP waveguides as a function of polymer film thickness. It can be seen that the ASE wavelength blue-shifts 15 nm, while the threshold increases from 0.2 μJ to 4 μJ when the thickness of the film is reduced from 68 nm to 40 nm.

The gain characteristics of the waveguides were measured with the variable stripe length method [23]. The light intensity emitted from the waveguides as a function of excitation stripe length was recorded for a range of different pump energies. Note that in all cases the polymer layer was thick enough to support a propagating mode at the gain maximum. For shorter stripe lengths the output signal grows exponentially, as expected for ASE. For longer stripe lengths, due to the high net gain of the polymer, saturation occurs. To calculate the gain coefficients, g, we fitted only those subsets of data for which gain saturation was not evident (i.e. the small signal regime). We have also studied the variation in the net gain coefficient for Dow Red F waveguides as the pump wavelength was tuned to the separate absorption features, $\lambda_{ex} = 337$ nm, 440 nm and 532 nm. It was found that the highest gain is obtained at $\lambda_{ex} = 532$ nm irrespective of the pump energy. The net gain coefficients, g, determined from these experiments for F8DP, PFO, F8BT and Red F waveguides are shown in Fig. 8 as a function of pump energy. It can be seen that the net gain increases more or less linearly up to a saturation value when plotted on a logarithmic pump energy scale. The maximum net gain coefficients and the observed saturation energy densities are given in Table 1 for each of the individual conjugated polymers that we have studied.

To more fully characterize the conjugated polymer waveguides that we have studied, we also measured their characteristic losses. These structures were the same ones used to measure the g values i.e. of sufficient polymer thickness to support a mode at the gain maximum. Fig. 9 shows the output light intensities at the respective ASE wavelengths as a function of the displacement of a fixed pump stripe (2 mm × 400 μm) from the sample edge. The pump energy was $\sim 5.0 \times E_{th}$ in each case. The data were fitted assuming an exponential dependence on length according to Eq. (2) and the loss coefficients extracted are listed in Table 1. The recorded losses of 3.2–14.8 cm^{-1} are very small for single component polymer films and are indicative of the excellent film forming properties of the polymers that we have studied. Factors that influence this loss include the relative confinement of the propagating mode within the polymer film (as opposed to the substrate), scattering from surface roughness and/or micro-void structures and the relative strength of any ground state absorption tail. The relatively high loss for

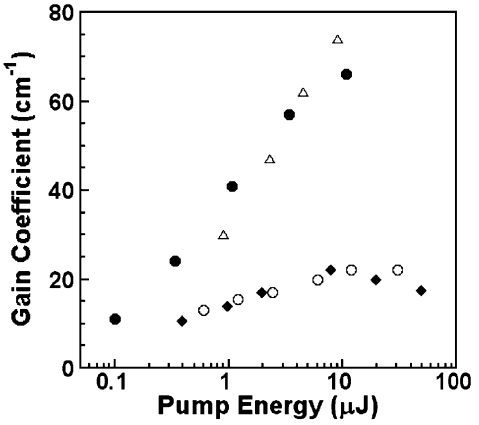

Fig. 8. Net gain coefficients as a function of pump energy for F8DP (●), PFO (△), F8BT (◆) and Red F (○) waveguides.

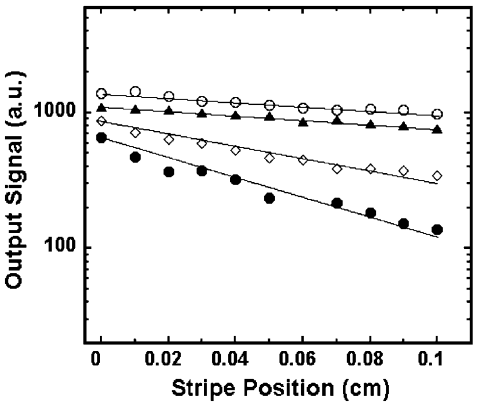

Fig. 9. Dependence of the emission intensity at λ_{ASE} on the length of the unpumped region between the edge of the excitation stripe and the substrate edge of the waveguide: F8DP (●), PFO (▲), F8BT (◇) and Dow Red F (○).

F8DP may be due to a larger overlap between its absorption and emission spectra (smaller Stokes shift) and/or due to greater mode confinement. Further experiments will address this question.

As a final test of our conjugated polymers as gain materials, we fabricated optically pumped surface emitting distributed feedback (DFB) lasers. The thin-film slab waveguide samples described above are not lasers because they do not have a resonant cavity structure to provide the necessary feedback to generate discrete lasing modes defined by the cavity geometry. In our DFB structures, we introduced resonant feedback by spin coating the polymer films onto gratings patterned into silica substrates. Optically pumped surface emission lasers were demonstrated using F8DP, PFO and Dow Red F [33,34]. By varying the grating period and polymer film thickness, we were able to systematically vary the lasing wavelength over a tuning range of at least 40 nm in the blue and 60 nm in the red. PFO DFB lasers with two-dimensional gratings had pump pulse energy thresholds as low as 0.8 nJ (with an excitation area of 250×100 μm^2) and slope efficiencies of up to 8% both of which represent the current state of the art for conjugated polymer DFB lasers: Further details will be reported elsewhere [35] and further optimization of performance is on-going.

4. Discussion

The ease with which ASE can be achieved for the polymers we have studied and their good performance in DFB lasers is a consequence of a combination of attractive features that are characteristic for conjugated polymers:

(i) They have large absorption coefficients, $\alpha \approx 10^5$ cm^{-1}, and consequently large cross-sections for stimulated emission,
(ii) They have high PLQE values in the solid state unlike many laser dyes for which there is strong concentration quenching,
(iii) There is a spectral separation between the absorption and emission (Stokes' shift) that gives low ground state absorption at the maximum gain wavelength and ensures that, as long as scattering losses are kept low, the net gain can closely approach the gain determined by the stimulated emission cross-section ($g_{net} \approx g$),
(iv) They possess a quasi-four-vibronic-level structure at the wavelength of maximum gain that allows low thresholds for lasing.

Comparing the four pure materials, we note that F8DP slab waveguides exhibit lower E_{th} values than do the corresponding PFO waveguides. This is despite the fact that these two polymers exhibit very similar absorption and emission spectra and PLQE values. A comparison of the E_{th} values and the PL decay times, shows, however, that the lower E_{th} value for F8DP seemingly correlates with a longer PL lifetime. We also observed a lifetime increase when we blended Dow Red F with increasing amounts of F8BT, and there was a corresponding decrease in E_{th}. The PL lifetime correlation cannot, however, be the full explanation for the changes in E_{th} since there is a similar fractional increase in lifetime between F8BT and Dow Red F which does not lead to a lower E_{th}, although in this case the PLQE drops significantly as well. In addition, the F8DP waveguides have much larger losses than those for the PFO waveguides. Further studies are needed in order to adequately de-convolute the contributions from lifetime effects and those associated with differing degrees of propagating mode confinement within the conjugated polymer layer. Shorter pulse excitation (ps rather than ns) together with ellipsometry and optical modelling should be able to resolve this issue and is currently being undertaken [36].

A significant reduction of E_{th} was observed for F8BT and Dow Red F waveguides when the pump wavelength was tuned to the longer wavelength absorption peaks. We consider that this is an indication that energy transfer between the states responsible for the absorption peaks at 330 nm, 455 nm and 550 nm (Fig. 1(a)) is incomplete. With this assumption, comparison of E_{th} values for different pump wavelengths allows an estimate of the losses during non-radiative energy transfer from higher lying to lowest lying singlet states. The threshold energy E_{th} can be expressed as

$$E_{th} = \frac{hc}{\lambda_{ex}} N_{ex}, \tag{3}$$

where λ_{ex} is the pump wavelength, c is the speed of light in vacuum, h is Planck's constant, and N_{ex} is the number of excitation photons that contribute to the ASE process: $N_{ex} \leqslant$ the number of photons that are absorbed. Since the absorption strength of F8BT (and Red F) is almost the same value at $\lambda_{ex} = 337$ nm and $\lambda_{ex} = 440$ nm (see Fig. 1(a)), the difference in E_{th} when pumping at these two wavelengths can be considered due to a loss of excitations during non-radiative transfer between the states responsible for the peaks at 330 nm and 455 nm. Using Eq. (3) we compared the effective number of excitation photons, $N_{ex}^{337\text{ nm}}$ and $N_{ex}^{440\text{ nm}}$ required for the measured E_{th} at $\lambda_{ex} = 337$ nm and $\lambda_{ex} = 440$ nm for F8BT waveguides. The E_{th} values are 1.1 μJ for $\lambda_{ex} = 337$ nm and 0.45 μJ for $\lambda_{ex} = 440$ nm. Accounting for the difference in wavelength, we obtained $N_{ex}^{440\text{ nm}} = 0.53\ N_{ex}^{337\text{ nm}}$. This result suggests that about 47% of the effective excitations are lost during the non-radiative relaxation following pumping at 337 nm.

We estimated the loss during energy transfer between the states responsible for the peak at 455 nm and the shoulder at 550 nm for Dow Red F in the same way. Fig. 1(a) shows that the absorption strength at 440 nm is some 7.23 times stronger than at 532 nm. However, E_{th} (see Fig. 4) is 0.45 μJ for both $\lambda_{ex} = 440$ nm and 532 nm. Again, accounting for the difference in wavelength, the E_{th} values suggest that about 83% of the effective excitations are lost during the non-radiative relaxation following pumping at 440 nm. This result suggests that it will be essential to increase the energy transfer efficiency in order to realize a low E_{th} value in such copolymer waveguides. We note that the ASE linewidths well above threshold do not show any differences when the waveguides are pumped with either of these two wavelengths. This gives confidence that the comparison of E_{th} values is a reasonable procedure.

As an additional characterization we have calculated the polymer refractive index (n_p) at the wavelength of maximum net gain for each polymer waveguide. Below a cut-off point, at which the film can no longer support a propagating mode at the wavelength of maximum gain, the ASE wavelength shows a strong dependence on the thickness of the film (see Section 3). For the zero-order transverse electric (TE_0) mode, the waveguide cut-off thickness, d_c, can be expressed as

$$d_c^{TE_0} = \frac{\lambda}{2\pi\sqrt{n_p^2 - n_s^2}} \arctan\left(\sqrt{\frac{n_s^2 - n_c^2}{n_p^2 - n_s^2}}\right), \tag{4}$$

where n_p, n_s and n_c are the refractive indices of the polymer, substrate (Spectrosil B) and cladding (air) layers, respectively, and λ is the wavelength of the guided light [37]. From Eq. (4), we can estimate the effective refractive indices of the polymer waveguide structures, using the measured d_c values (listed in Table 1) together with the known values of the other parameters, namely $n_c = 1.0$ and $n_s = 1.466$, 1.464, 1.459 and 1.456 at $\lambda = 466$ nm, 452 nm, 576 nm and 686 nm respectively. The calculated refractive indices for the four polymers are listed in Table 1.

Finally, the gain cross-sections were calculated from the measured saturation energy densities E_S/A, using the expression

$$\frac{E_S}{A} = \frac{hc}{\lambda\sigma}, \tag{5}$$

where E_S is the pulse energy at which saturation occurs, A is the pump stripe area, namely 0.04×0.4 cm^2 for our experimental set up, and λ is the ASE peak wavelength. The measured saturation energy densities, E_S/A, are reported in Table 1. Using Eq. (5), we estimate an order of magnitude for the gain cross-section, $\sigma \approx 7 \times 10^{-16}$ cm^2 for all of the conjugated polymers studied in this work (see Table 1 for specific values). Errors in determining the saturation excitation density limit the accuracy of this value. It is, however, comparable with those reported for polyparaphenylenevinylene (1×10^{-16} cm^2) [5], a range of dialkoxy and dialkyl substituted phenylenevinylene and phenyleneethynylene polymers ($\leqslant 2 \times 10^{-16}$ cm^2) [38], and for established laser dyes such as Rhodamine 6G (2×10^{-16} cm^2). A cross-section $\sigma \approx 7 \times 10^{-16}$ cm^2 leads to an expected gain coefficient $g \approx 70$ cm^{-1} for $N_{ex} = 10^{17}$ cm^{-3}, in good agreement with our experimental results.

5. Conclusions

We have presented a detailed study of the gain properties of four polyfluorenes, namely poly(9,9-dioctylfluorene), poly(9,9-dioctylfluorene-*co*-9,9-di(4-methoxy)phenylfluorene), poly(9,9-dioctylfluorene-*co*-benzothiadiazole), and a Dow proprietary red emission copolymer, Dow Red F. The emission spectra of these four materials span the range from 400 to 800 nm, covering the full visible spectrum. Efficient light amplification was demonstrated at 452 nm, 466 nm, 576 nm and 685 nm via ASE in optically pumped planar asymmetric waveguides containing F8DP, PFO, F8BT and Dow Red F, respectively. The E_{th} values can be reduced by both orientation to control the allowed waveguide modes and by preparing blends of the emissive component in a wider optical gap host matrix. In the latter case, blends of Dow Red F in F8BT show a decrease by an order of magnitude from the E_{th} values of the neat polymer films. The ASE wavelength can be tuned across a range of 20–29 nm by changing the thickness of the waveguides or, again by preparing blends (e.g. Dow Red F in F8BT). The cut-off thickness values for individual polymer waveguides were determined and used to calculate the refractive indices of polymers contained therein. Variable stripe length gain measurements show large net gains of up to 74 cm^{-1} at the peak ASE wavelength with gain cross sections of $6.6 \times 10^{-16} \leqslant \sigma \leqslant 7.8 \times 10^{-16}$ cm^2. Very low loss coefficients were also determined, namely $15 \geqslant \alpha \geqslant 3$ cm^{-1}, from waveguide propagation experiments. Our investigations clearly demonstrate that fluorene-based polymers are suitable as high gain media for tuneable solid-state lasers that emit at wavelengths across the full visible spectrum.

As already noted above, progress towards electrically pumped amplifiers and lasers will require additional studies focussed on the polymer electrode interactions, the rôle of injected charges and resulting triplet states in reducing gain through intra-gap absorption and their contributions to degradation. The need to reduce unfavourable inter-chain interactions has been highlighted by the studies on Dow Red F/F8BT blends and the generality of such interactions is worth significant additional attention [39]. Further efforts to enhance charge carrier mobilities are also needed as progress in this area may allow a larger separation of electrodes and hence reduced interaction with the propagating mode at the peak gain wavelength. The stimulated emission lifetime is also important for any approach towards continuous wave operation: This is typically of order 10 ps or less but can be as much as 60 ps [40]. Even longer times are desirable. Progress is still possible on all of these areas and hence the electrically pumped polymer laser remains a suitable challenge for on-going research.

Acknowledgements

The authors thank Mark Bernius, Rob Fletcher, Mike Inbasekaran, and Jim O'Brien of The Dow Chemical Company for providing the four polymers that we have studied in our experiments. We are also grateful to the United Kingdom Engineering and Physical Sciences Research Council (Ultrafast Photonics Collaboration GR/R55078) for financial support. Finally, we acknowledge experimental assistance from Dr. Mattijs Koeberg and useful discussions with Mariano Campoy-Quiles.

References

[1] F. Hide, M.A. Diaz-Garcia, B.J. Schwartz, M.R. Andersson, P. Qibing, A.J. Heeger, Science 273 (1996) 1833.
[2] R.H. Friend, R.W. Gymer, A.B. Holmes, J.H. Burroughes, R.N. Marks, C. Taliani, D.D.C. Bradley, D.A. Dos Santos, J.L. Brédas, M. Lögdlund, W.R. Salaneck, Nature 397 (1999) 121.
[3] S.V. Frolov, W. Gellermann, M. Ozaki, K. Yoshino, Z.V. Vardeny, Phys. Rev. Lett. 78 (1997) 729.
[4] N. Tessler, Adv. Mater. 11 (1999) 363.
[5] U. Scherf, S. Riechel, U. Lemmer, R.F. Mahrt, Curr. Opin. Solid State Mat. Sci. 5 (2001) 143.
[6] M.D. McGehee, A.J. Heeger, Adv. Mater. 12 (2000) 1655.
[7] D. Moses, Appl. Phys. Lett. 60 (1992) 3215.
[8] W. Holzer, A. Penzkofer, S.H. Gong, A. Bleyer, D.D.C. Bradley, Adv. Mater. 8 (1996) 974.
[9] S.V. Frolov, A. Fujii, D. Chinn, Z.V. Vardeny, K. Yoshino, R.V. Gregory, Appl. Phys. Lett. 72 (1998) 2811.
[10] N. Tessler, G.J. Denton, R.H. Friend, Nature 382 (1997) 695.

[11] M.D. McGehee, M.A. Diaz-Garcia, F. Hide, R. Gupta, E.K. Miller, D. Moses, A.J. Heeger, Appl. Phys. Lett. 72 (1998) 1536.
[12] G. Heliotis, D.D.C. Bradley, G.A. Turnbull, I.D.W. Samuel, Appl. Phys. Lett. 81 (2002) 415.
[13] T.-W. Lee, O. Ok Park, D.H. Choi, H.N. Cho, Y.C. Kim, Appl. Phys. Lett. 81 (2002) 424.
[14] G.A. Turnbull, P. Andrew, M.J. Jory, W.L. Barnes, I.D.W. Samuel, Phys. Rev. B 64 (2001) 125122.
[15] B.J. Schwartz, F. Hide, M.R. Andersson, A.J. Heeger, Chem. Phys. Lett. 256 (1997) 327.
[16] M. Redecker, D.D.C. Bradley, M. Inbasekaran, E.P. Woo, Appl. Phys. Lett. 73 (1998) 1565;
M. Redecker, D.D.C. Bradley, M. Inbasekaran, E.P. Woo, Appl. Phys. Lett. 74 (1999) 1400.
[17] A.J. Campbell, D.D.C. Bradley, H. Antoniadis, Appl. Phys. Lett. 79 (2001) 2133.
[18] V.G. Kozlov, G. Parthasarathy, P.E. Burrows, V.B. Khalfin, J. Wang, S.Y. Chou, S.R. Forrest, IEEE J. Q. E. 36 (2000) 18.
[19] M.A. Baldo, R.J. Holmes, S.R. Forrest, Phys. Rev. B 66 (2002) 035321.
[20] J.C. de Mello, H.F. Wittmann, R.H. Friend, Adv. Mater. 9 (1997) 230.
[21] N.C. Greenham, I.D.W. Samuel, G.R. Hayes, R.T. Phillips, Y.A.R.R. Kessener, S.C. Moratti, A.B. Holmes, R.H. Friend, Chem. Phys. Lett. 24 (1995) 89.
[22] Y. Hou, M. Koeberg, D.D.C. Bradley, Synth. Met. 139 (2003) 859.
[23] K.L. Shaklee, R.F. Leheny, Appl. Phys. Lett. 18 (1971) 475.
[24] M.D. McGehee, R. Gupta, S. Veenstra, E.K. Miller, M.A. Diaz-Garcia, A.J. Heeger, Phys. Rev. B 58 (1998) 7035.
[25] M. Sims, M. Ariu, A. Asimakis, M. Koeberg, M. Stouff, M. Fox, D.D.C. Bradley, Proc. SPIE (2003) in press.
[26] M. Grell, D.D.C. Bradley, G. Ungar, J. Hill, K. Whitehead, Macromolecules 32 (1999) 5810.
[27] A.J. Cadby, P.A. Lane, H. Mellor, S.J. Martin, M. Grell, C. Giebeler, D.D.C. Bradley, Phys. Rev. B 62 (2000) 15604.
[28] V.G. Kozlov, V. Bulovic, P.E. Burrows, S.R. Forrest, Nature 389 (1997) 362.
[29] H. Liem, P. Etchegoin, K.S. Whitehead, D.D.C. Bradley, Adv. Funct. Mater. 13 (2003) 66.
[30] X. Long, M. Grell, A. Malinowski, D.D.C. Bradley, M. Inbasekaran, E.P. Woo, Opt. Mater. 9 (1998) 70.
[31] G. Heliotis, R. Xia, K.S. Whitehead, G.A. Turnbull, I.D.W. Samuel, D.D.C. Bradley, Synth. Met. 139 (2003) 727.
[32] R. Xia, G. Heliotis, Y. Hou, D.D.C. Bradley, Chem. Phys. Lett. (2003) in press.
[33] G. Heliotis, R. Xia, G.A. Turnbull, P. Andrew, W.L. Barnes, I.D.W. Samuel, D.D.C. Bradley, Adv. Funct. Mater. (2003) in press.
[34] G. Heliotis, R. Xia, D.D.C. Bradley, G.A. Turnbull, I.D.W. Samuel, P. Andrew, W.L. Barnes, Appl. Phys. Lett. 83 (2003) 2118.
[35] R. Xia, G. Heliotis, G.A. Turnbull, I.D.W. Samuel, P. Andrew, W.L. Barnes, D.D.C. Bradley, Proc. MRS Vol. 771 (2003) in press.
[36] M. Campoy-Quiles, G. Heliotis, R. Xia, M. Ariu, M. Pintani, P. Etchegoin, D.D.C. Bradley, unpublished.
[37] M. Marcuse, Theory of Dielectric Waveguides, Academic, New York, 1974, Chap. 1.
[38] W. Holzer, M. Pichlmaier, A. Penzkofer, D.D.C. Bradley, W.J. Blau, Chem. Phys. 246 (1999) 445.
[39] R. Gupta, M. Stevenson, A. Dogariu, M.D. McGehee, J.Y. Park, V. Srdanov, A.J. Heeger, Appl. Phys. Lett. 73 (1998) 3492.
[40] B.J. Schwartz, F. Hide, M.R. Andersson, A.J. Heeger, Chem. Phys. Lett. 265 (1997) 327.